ACS APPLIED MATERIALS & INTERFACES

Letter

www.acsami.org

Aligned Nanofibers as an Interfacial Layer for Achieving High-Detectivity and Fast-Response Organic Photodetectors

Riming Nie,[†] Yangyang Wang,[†] and Xianyu Deng*[,†]

[†]Research Center for Advanced Functional Materials and Devices, Shenzhen Engineering Lab of Flexible Transparent Conductive Films, Shenzhen Key Laboratory of Advanced Materials, School of Materials Science and Engineering, Shenzhen Graduate School, Harbin Institute of Technology, 518055 Shenzhen, P. R. China

Supporting Information

ABSTRACT: We report that aligned nanofibers (ANs) prepared by electrostatic spinning technology as an interfacial layer can significantly enhance the performance of inverted organic photodetectors. With the insertion of ANs of titanium dioxide (TiO_2), the optimized organic photodetectors had a highest detectivity of 2.93×10^{13} Jones at zero bias, which is about 3 times higher than that of a similar organic photodetector without ANs and also markedly higher than that of traditional silicon photodetectors. The performance of the devices with different TiO_2 ANs as the interfacial layer was investigated, and the results exhibited that photodetectors with one-way ANs had the highest detectivity and shortest response time. This work provides a new application of nanofibers fabricated by a simple and controllable process in high-performance organic photodetectors.

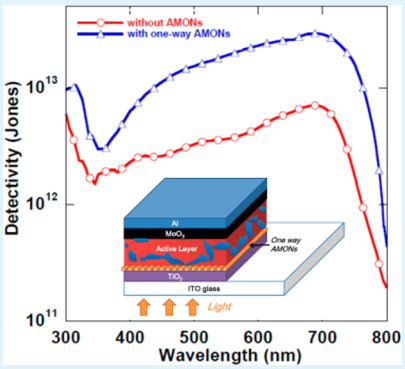

KEYWORDS: *nanofibers, photodetectors, organic electronics, interfacial modification*

INTRODUCTION

With the rapid and productive development of nanoscience and nanotechnology, research has been focused toward developing materials with novel nanostructures to realize various functional applications.[1−7] One important direction of the research is creating nanostructures with especially excellent optical and electrical properties for use in optoelectronic devices. As one kind of optoelectronic device, organic-based photodetectors (OPDs) have been attracting considerable interest during the past years because of their inherent advantages compared with the traditional photodetectors with inorganic materials. These advantages include the wide source of materials, the ease of process, and the low-cost, flexible, large-scale, and high-resolution fabrication of devices. This gives them promising potential for use in a number of important areas, including optical detection, imaging, and communications.[8−11] An appropriate interfacial layer that enables photoinduced holes and electrons to be transferred effectively from an active layer to an electrode is very important to obtain a high-performance organic photodetector. Valouch et al. demonstrated that the introduction of a hole interfacial layer prepared from a small molecular solution can improve the dark current characteristics of polymer photodiodes.[12] Keivanidis et al. demonstrated a dark current reduction down to few tens of nanoamperes per centimeters squared in an all-solution-processed P3HT:F8TBT-based OPD by the introduction of dedicated collection layers both at the anode side and at the cathode side, respectively.[13] Gong et al. reported that photodetectors based on the bulk-heterojunction structure of a low-band-gap polymer PDDTT blend with $PC_{61}BM$ exhibited a specific detectivity higher than 10^{12} Jones at a wavelength of 800 nm by inserting spin-coated polystyrene−*N*,*N*-diphenyl-*N*,*N*-bis(4-nbutylphenyl)-1,10-biphenyl-4,4-diamine−perfluorocyclobutane (PS−TPD−PFCB) as the hole collection layer and thermally evaporated C_{60} as the electron collection layer.[14] Even with those, the performances of the detectivity, response speed, and stability of the OPDs still require full-scale improvement for their commercial applications.

Nanofibers produced by electrospinning technology have been widely investigated during the past decades because of their ease of production and various applications in key areas such as chemical sensors,[15] supercapacitors,[16] mechanical and electrical devices,[17,18] and tissue engineering.[19,20] In these nanofibers, some made from n-type metal oxide semiconductors of zinc oxide (ZnO) and titanium dioxide (TiO_2) have aroused much interest because it was found that they could be used as excellent electron collection and transport materials in organic and organic−inorganic hybrid optoelectric devices.[21−32] The performance of these optoelectric devices has been significantly enhanced by the use of nanofibers. One of the primary advantages of electrospinning technology is that it has the ability to accurately control the direction and size of the nanofibers of a variety of materials. This makes it easy to achieve aligned nanofibers (ANs) of metal oxides such as ZnO

Received: April 1, 2014
Accepted: May 1, 2014
Published: May 1, 2014

and TiO_2. These ANs are very likely to have better optical and electrical properties, such as electron mobility and light transmission, than those of the corresponding nanofibers with unordered state. This means that they are more promising for being able to significantly enhance the performance of devices in optoelectronic applications. However, to our knowledge, so far none of the ANs produced by electrospinning processes have been explored in the fabrication of organic photodetectors.

Here, we demonstrated high-detectivity and fast-response OPDs by the insertion of aligned metal oxide nanofibers (AMONs) of TiO_2 as an interfacial layer. In the organic photodetectors, the blend of thieno[3,4-*b*]thiophene/benzodithiophene (PTB7) and [6,6]phenyl C_{71}-butyric acid methyl ester ($PC_{71}BM$) was used as a photoactive layer. The device with a layer of the aligned TiO_2 nanofiber had a significantly increased detectivity, as well as a largely shortened response time. The devices with random, multiway, or one-way aligned TiO_2 nanofibers as the interfacial layer were comparably investigated, which demonstrated that the device with the one-way AMONs of TiO_2 exhibited the best performance.

RESULTS AND DISCUSSION

Figure 1a shows the chemical structures of PTB7 and $PC_{71}BM$, and Figure 1b shows the device structure of the photodetectors.

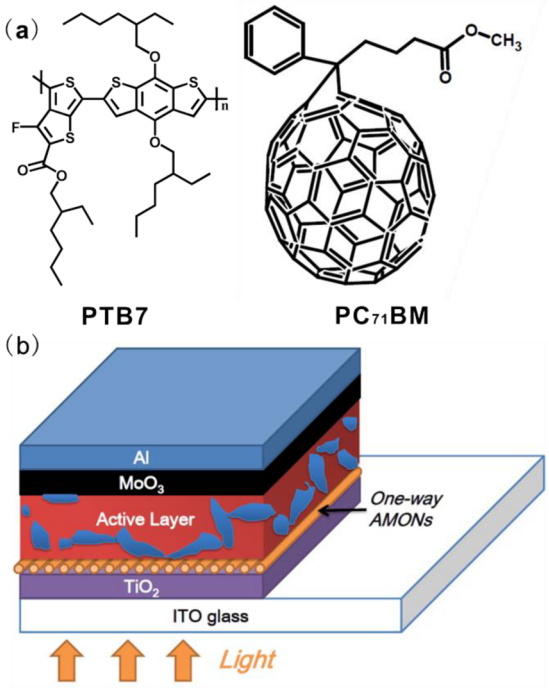

Figure 1. (a) Molecular structures of PTB7 and $PC_{71}BM$. (b) Device architecture of the OPD with one-way AMONs of TiO_2 as the electron collection layer.

Parts a and b of Figure 2 show the current−voltage (I−V) characteristics of OPDs without AMONs of TiO_2 or with one-way AMONs of TiO_2, respectively. Both OPDs showed a rectification ratio near 1.0×10^4 at a bias voltage of ±2 V, indicating excellent diode characteristics of the two devices. At a bias voltage of 0 V, the device with one-way AMONs had a current density in the darkness about 2.5 times lower than that of the device without AMONs. Conversely, the photocurrent density of the device with one-way AMONs was about 3.0 times higher than that of the device without AMONs at a wide range of bias from 0 to −2.0 V. With a result similar to that of the photocurrent, the external quantum efficiency (EQE), as shown in Figure 2c, was also significantly enhanced by adding a layer of one-way AMONs. At a wavelength of 690 nm, EQE was 35.60% for the device without AMONs and 94.22% for the device with one-way AMONs. These results lead to a significant enhancement of the detectivity of the device with one-way AMONs compared to the device without AMONs, which is shown in Figure 2d. At a wavelength of 690 nm, the detectivity increased from 7.05×10^{12} to 2.93×10^{13} Jones, while one-way AMONs were inserted. The OPD with one-way AMONs of TiO_2 as an interfacial layer exhibited a detectivity higher than 10^{13} Jones in a wide absorption range from 440 to 760 nm. The result is nearly the highest detectivity in previous reports, which is remarkably higher than that of conventional inorganic silicon-based photodetectors.[33] The EQEs of these OPDs under different reverse voltages are shown in Figure S1 in the Supporting Information (SI). The result shows that the EQE value is higher than 100% at a higher bias voltage. A second carrier emission under a high biasing field could contribute over 100% quantum yield.[34,35] Even though it is not clear what the detailed mechanism is, these devices appear promising for use in practical applications because of the high response (or quantum efficiency).

Figure 3a shows the response of a device's photovoltage (V_{rp}) against time, while the device was illuminated under a red laser diode with a frequency of 20 kHz. Both the device without AMONs of TiO_2 and the device with one-way AMONs of TiO_2 had a short response time at the level of microseconds. The rise time (T_r, the time it took the V_{rp} value to rise from 10% to 90%) and the decay time (T_d, the time it took the V_{rp} value to fall from 90% to 10%) of the device without AMONs were 10.8 and 11.2 μs, respectively, while those of the devices with one-way AMONs of TiO_2 were 2.3 and 5.8 μs, respectively. Figure 3b shows the frequency response curve of these devices under short-circuit conditions. With one-way AMONs of TiO_2, the −3 dB bandwidth of the OPDs increases from 3.25×10^4 to 1.54×10^5 Hz. These results from the response of a device's V_{rp} against time and frequency response indicated that the device with one-way AMONs of TiO_2 had a faster response speed than the device without the insertion of AMONs. Figure 3c shows the −3 dB bandwidth of the OPDs without or with one-way AMONs of TiO_2 under different reverse voltages. With the reverse voltage changing from −2 to −7 V, the bandwidth increases from 3.20×10^4 to 6.50×10^4 Hz for OPDs without AMONs of TiO_2, while it increases from 1.54×10^5 to 5.99×10^5 Hz for OPDs with one-way AMONs of TiO_2. The increase of the −3 dB bandwidth of the device with one-way AMONs of TiO_2 is near 3 times that of the device without the interfacial layer. This result indicated that the response speed of devices with one-way AMONs of TiO_2 is more obviously improved at high reverse voltage. Figure 3d shows capacitance−voltage characteristics of the two OPDs. The capacitance of the OPD without AMONs of TiO_2 was almost constant at the reverse bias between −5 and −0.35 V, while that of the OPD with one-way AMONs of TiO_2 is constant at the bias between −5 and +0.35 V. This indicates that fast response speeds can be achieved even at zero or lower positive biasing voltages for the device with one-way AMONs of TiO_2, while it can be realized only at negative bias for the device without the AMONs.[36]

To investigate the effect of the inserted TiO_2 nanofibers with different alignments on the performance of OPDs, we prepared

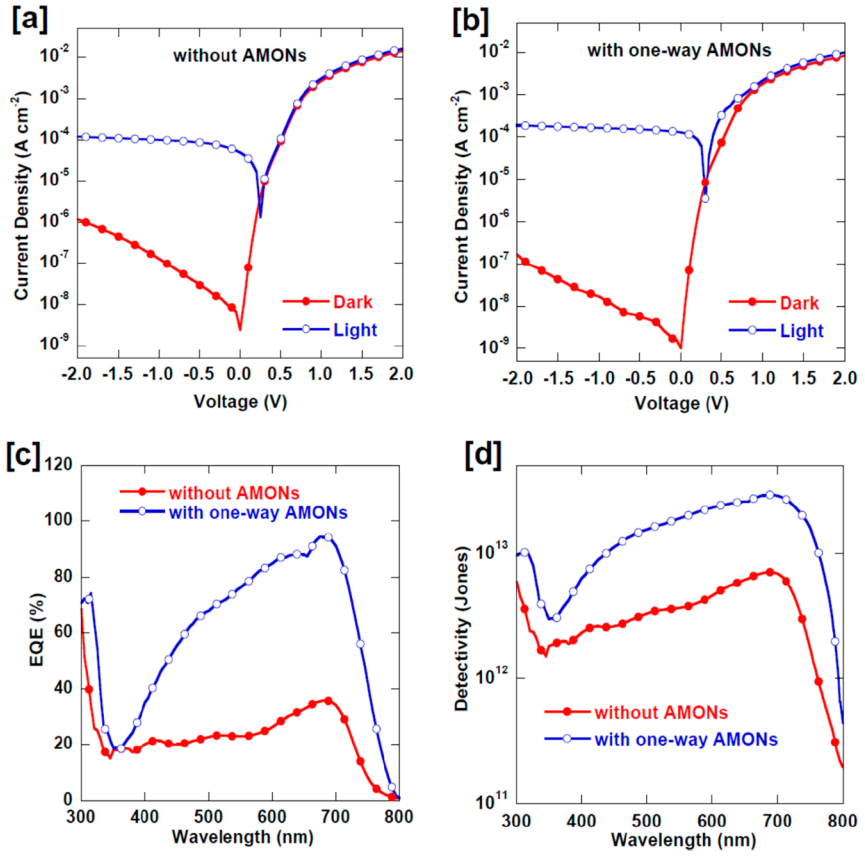

Figure 2. $I-V$ characteristics of the OPDs (a) without AMONs of TiO_2 or (b) with one-way AMONs of TiO_2 measured in the dark and under illumination (λ = 650 nm) with a light intensity of 0.25 mW cm^{-2}. (c) EQE and (d) detectivities versus the wavelength under short circuits of OPDs without AMONs of TiO_2 or with one-way AMONs of TiO_2.

three different TiO_2 nanofibers for use as an electron collection layer in the photodetector devices. Figure 4 shows the scanning electron microscopy (SEM) images of one-way AMONs of TiO_2, multiway AMONs of TiO_2, and random AMONs of TiO_2. The diameters of TiO_2 nanofibers with all of these alignments are mostly between 200 and 300 nm. The performance of the devices using these three different AMONs of TiO_2 is summarized in Table 1. From Table 1, the device with one-way AMONs of TiO_2 exhibited the lowest dark current and the highest photocurrent, EQE, and detectivity. The reason for the results should be associated with the ability of charge separation from the active layer into the interfacial layer. According to a previous report,[37] with the alignment degree of the TiO_2 nanofibers increasing, the photoluminescence intensity of polymer/TiO_2 systems was significantly decreased, which indicates that TiO_2 with high order formation could accelerate charge separation at the inorganic–organic interface. Similarly, the response speed of the device can also be enhanced by suppressing the charge recombination and facilitating the charge transportation.[38] Therefore, the fast transfer of the electron between the organic layer and the TiO_2 layer also lead to the fast response speed of the OPDs with one-way aligned TiO_2. To further investigate the reason why AMONs of TiO_2 have better charge separation at the interface and charge transport within the interfacial layer, X-ray diffraction (XRD) of one-way AMONs of TiO_2, multiway AMONs of TiO_2, and random AMONs of TiO_2 was measured, and the results are shown in Figure 4d. From the XRD spectra, one-way AMONs of TiO_2 exhibited a better crystallization than the other two AMONs of TiO_2. The electric field force at a fixed direction during the preparation of AMONs of TiO_2 caused the polymer main chain to arrange and accumulate more compactly toward one direction, resulting in crystallization of TiO_2 occurring more easily. The semiconductor of metal oxide with good crystallization not only has a good charge-transport property but also can facilitate charge separation at the organic–inorganic interface because the trap density induced by defects is markedly reduced in it.[39]

The stability of the OPDs was investigated by measuring how changes in the maximum photoresponse voltage (V_{mrp}) and rise time (T_r) of the devices depended on the times that they were electrically read. Measurements were carried out on conditions that the devices were exposed to air without any encapsulations and illuminated under a pulse monochromatic light with a wavelength of 650 nm, an intensity of 0.25 mW cm^{-2}, and a frequency of 10^4 Hz. Figure 5 shows the delay of V_{mrp} and T_r of the OPDs without AMONs of TiO_2 or with one-way AMONs of TiO_2. Both devices displayed less of a change in V_{mrp} and T_r after they were read a large number of times at 10^8. With the read times increased to 10^9, V_{mrp} and T_r of the device without AMONs of TiO_2 were decreased from 84 to 78 mV and increased from 10.8 to 13.1 μs, respectively. When the read times were increased to 10^{10}, V_{mrp} and T_r of the OPDs without AMONs of TiO_2 were decreased to a low value of 62 mV and increased to a high value of 14.2 μs. However, there was no obvious change in V_{mrp} and T_r for devices with one-way AMONs of TiO_2 even after they were electrically read up to

dx.doi.org/10.1021/am501977w | ACS Appl. Mater. Interfaces 2014, 6, 7032–7037

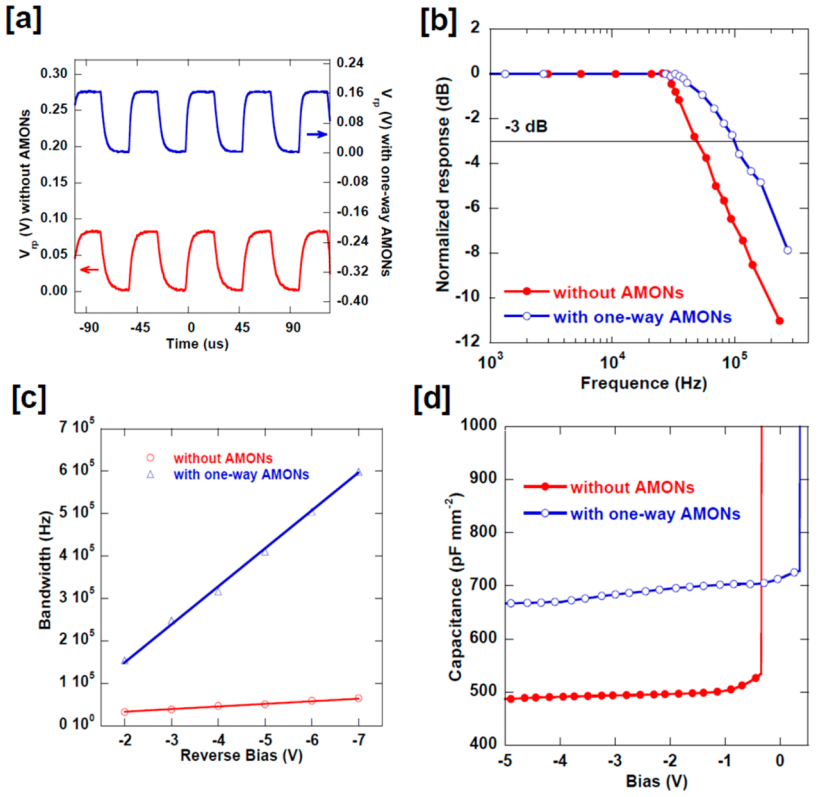

Figure 3. (a) Transient response under short-circuit conditions of the OPDs without AMONs of TiO_2 or with one-way AMONs of TiO_2 under 20-kHz-modulated 650 nm monochromatic illumination. V_{rp} is for the device's photovoltage. (b) Frequency response under short-circuit conditions of the OPDs under 650 nm monochromatic illumination with different frequencies. (c) −3 dB bandwidth of the OPDs without AMONs of TiO_2 or with one-way AMONs of TiO_2 under different reverse voltages. (d) Capacitance−voltage measurements of the OPDs at a frequency of 10 kHz.

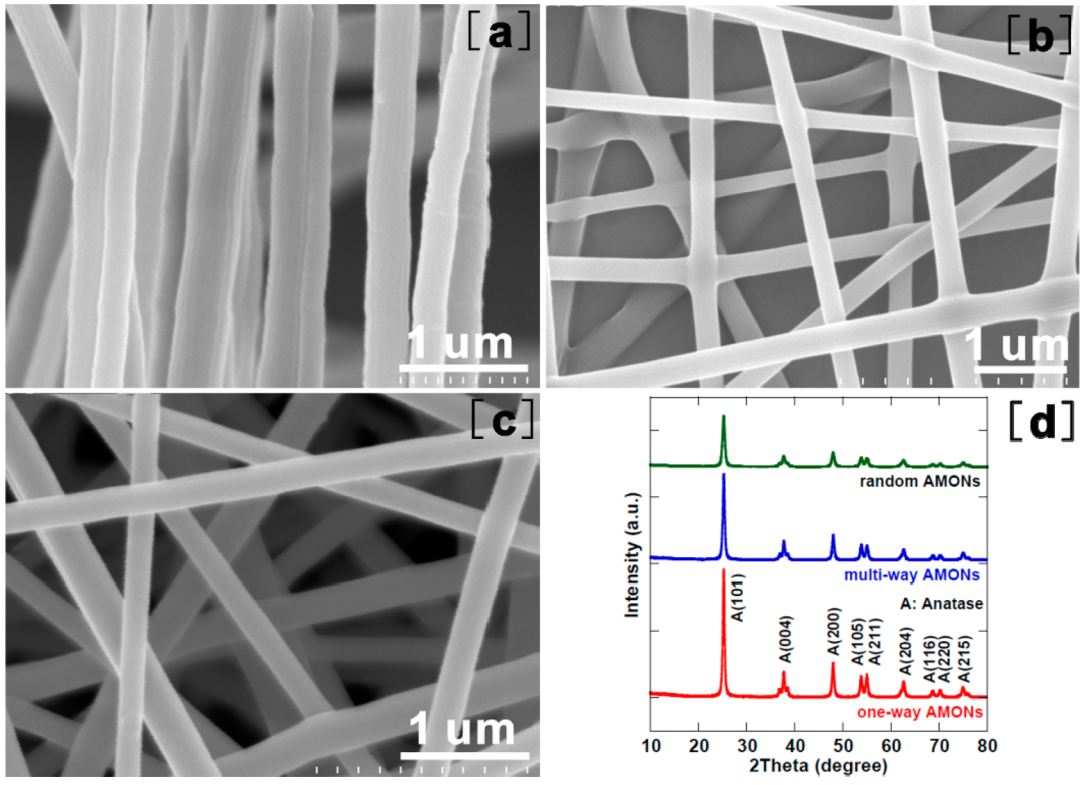

Figure 4. SEM images of (a) one-way AMONs of TiO_2, (b) multiway AMONs of TiO_2, and (c) random AMONs of TiO_2. (d) Typical XRD patterns of multiway AMONs of TiO_2, one-way AMONs of TiO_2, and random AMONs of TiO_2. One-way AMONs of TiO_2 and multiway AMONs of TiO_2 are highly aligned.

dx.doi.org/10.1021/am501977w | ACS Appl. Mater. Interfaces 2014, 6, 7032−7037

Table 1. Performance of OPDs with One-Way AMONs of TiO_2, Multiway AMONs of TiO_2, or Random AMONs of TiO_2 as the Electron Collection Layer at Wavelength = 690 nm under Short-Circuit Conditions

TiO_2 nanofibers	J_{dark}[a] (A cm^{-2})	J_{ph}[b] (A cm^{-2})	EQE (%)	R[c] (A W^{-1})	D^*[d] (Jones)
one-way AMONs	1.01×10^{-9}	1.28×10^{-4}	94.22	0.52	2.93×10^{13}
multiway AMONs	1.34×10^{-9}	1.17×10^{-4}	89.06	0.50	2.42×10^{13}
random AMONs	1.89×10^{-9}	1.03×10^{-4}	86.41	0.48	1.96×10^{13}

[a]Dark current. [b]Photocurrent. [c]Responsiveness. [d]Detectivity.

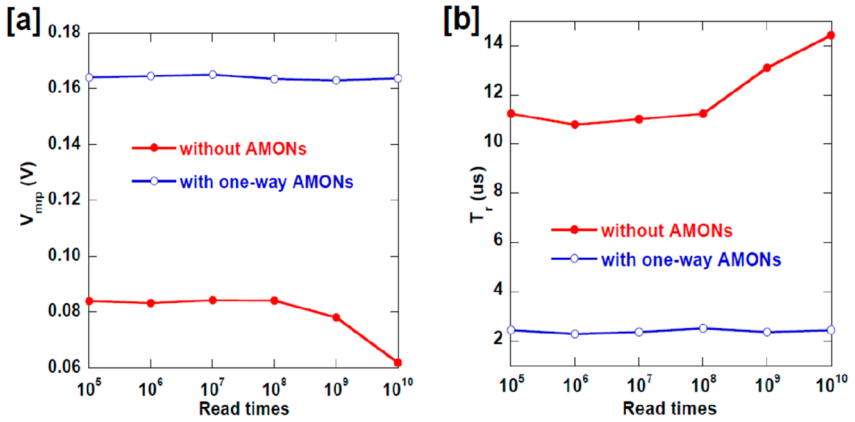

Figure 5. Changes of (a) the maximum photoresponse voltage (V_{mrp}) and (b) rise time (T_r) of the devices without AMONs of TiO_2 or with one-way AMONs of TiO_2 depending on the times that they were electrically read under illumination of a pulse monochromatic light with a wavelength of 650 nm, an intensity of 0.25 mW cm^{-2}, and a frequency of 10^4 Hz.

10^{10} times. The high stability indicates that the OPDs will easily realize commercial applications.

CONCLUSION

In conclusion, we have demonstrated the high detectivity and fast response of OPDs by inserting AMONs of TiO_2 as an electron collection layer. With one-way AMONs of the TiO_2 layer, PTB7:$PC_{71}BM$-based OPDs exhibited the highest detectivity of 2.93×10^{13} at zero bias and the shortest rise time of 2.3 μs. The enhancement of the performance was attributed to better crystallization of one-way AMONs of TiO_2, which facilitate charge separation at the organic−inorganic interface and electron transport within the interfacial layer. This work provides a pathway to the use of AMONs in fabricating high-performance OPDs.

ASSOCIATED CONTENT

Supporting Information

Experimental details, Table S1, and Figures S1−S4. This material is available free of charge via the Internet at http://pubs.acs.org.

AUTHOR INFORMATION

Corresponding Author

*E-mail: xydeng@hitsz.edu.cn. Tel: +86-755-26033211. Fax: +86-755-26033504.

Notes

The authors declare no competing financial interest.

ACKNOWLEDGMENTS

We acknowledge financial support from the Natural Scientific Research Innovation Foundation at the Harbin Institute of Technology (Grant 2009142) and the Shenzhen Research Foundation Project (Grants JC201005260119A, JC201105160573A, and JC201104220174A).

REFERENCES

(1) Poizot, P.; Laruelle, S.; Grugeon, S.; Dupont, L.; Tarascon, J.-M. Mn_3O_4−Graphene Hybrid as a High Capacity Anode Material for Lithium Ion Batteries. *Nature* **2000**, *407*, 496−499.

(2) Wang, X. D.; Summers, C. J.; Wang, Z. L. Large-Scale Hexagonal-Patterned Growth of Aligned ZnO Nanorods for Nano-Optoelectronics and Nanosensor Arrays. *Nano Lett.* **2004**, *4*, 423−426.

(3) Allen, C.; Maysinger, D.; Eisenberg, A. Nano-Engineering Block Copolymer Aggregates for Drug Delivery. *Colloids Surf., B* **1999**, *B16*, 3−27.

(4) Sun, X.; Liu, Z.; Welsher, K.; Robinson, J. T.; Goodwin, A.; Zaric, S.; Dai, H. Nano-Graphene Oxide for Cellular Imaging and Drug Delivery. *Nano Res.* **2008**, *1*, 203−212.

(5) Li, H.; Huang, X.; Chen, L.; Wu, Z.; Liang, Y. A High Capacity Nano Si Composite Anode Material for Lithium Rechargeable Batteries. *Electrochem. Solid State Lett.* **1999**, *2*, 547.

(6) Chen, Z.; Lin, Y. M.; Rooks, M. J.; Avouris, Ph. Graphene Nano-Ribbon Electronics. *Physica E* **2007**, *40*, 228−232.

(7) Yang, F.; Murugan, R.; Wang, S.; Ramakrishna, S. Electrospinning of Nano/Micro Scale Poly(L-lactic acid) Aligned Fibers and Their Potential in Neural Tissue Engineering. *Biomaterials* **2005**, *26*, 2603−2610.

(8) Konstantatos, G.; Howard, I.; Fischer, A.; Hoogland, S.; Clifford, J.; Klem, E.; Levina, L.; Sargent, E. H. Ultrasensitive Solution-cast Quantum Dot Photodetectors. *Nature* **2006**, *442*, 180−183.

(9) Sargent, E. H. Infrared Quantum Dots. *Adv. Mater.* **2005**, *17*, 515−522.

(10) Kim, S.; Lim, Y. T.; Soltesz, E. G.; De Grand, A. M.; Lee, J.; Nakayama, A.; Parker, J. A.; Mihaljevic, T.; Laurence, R. G.; Dor, D. M.; Cohn, L. H.; Bawendi, M. G.; Frangioni, J. Near-Infrared Fluorescent Type II Quantum Dots for Sentinel Lymph Node Mapping. *Nat. Biotechnol.* **2004**, *22*, 93−97.

(11) McDonald, S. A.; Konstantatos, G.; Zhang, S.; Cyr, P. W.; Klem, E. J. D.; Levina, L.; Sargent, E. H. Solution-processed PbS Quantum Dot Infrared Photodetectors and Photovoltaics. *Nat. Mater.* **2005**, *4*, 138−142.

(12) Valouch, S.; Hönes, C.; Kettlitz, S. W.; Christ, N.; Do, H.; Klein, M. F. G.; Kalt, H.; Colsmann, A.; Lemmer, U. Solution Processed

Small Molecule Organic Interfacial Layers for Low Dark Current Polymer Photodiodes. *Org. Electron.* **2012**, *13*, 2727−2732.
(13) Keivanidis, P. E.; Kong, S.-H.; Ho, P. K. H.; Greenham, N. C.; Friend, R. H. All-Solution Based Device Engineering of Multilayer Polymeric Photodiodes: Minimizing Dark Current. *Appl. Phys. Lett.* **2009**, *94*, 173303.
(14) Gong, X.; Tong, M.; Xia, Y.; Cai, W.; Moon, J. S.; Cao, Y.; Yu, G.; Shieh, C. L.; Nilsson, B.; Heeger, A. J. High-Detectivity Polymer Photodetectors with Spectral Response from 300 nm to 1450 nm. *Science* **2009**, *325*, 1665−1667.
(15) Liu, H. Q.; Kameoka, J.; Czaplewski, D. A.; Craighead, H. G. Polymeric Nanowire Chemical Sensor. *Nano Lett.* **2004**, *4*, 671−675.
(16) Kim, C.; Ngoc, B. T. N.; Yang, K. S.; Kojima, M.; Kim, Y. A.; Kim, Y. J.; Endo, M.; Yang, S. C. Self-Sustained Thin Webs Consisting of Porous Carbon Nanofibers for Supercapacitors via the Electrospinning of Polyacrylonitrile Solutions Containing Zinc Chloride. *Adv. Mater.* **2007**, *19*, 2341−2346.
(17) Kameoka, J.; Verbridge, S. S.; Liu, H. Q.; Czaplewski, D. A.; Craighead, H. G. Fabrication of Suspended Silica Glass Nanofibers from Polymeric Materials Using a Scanned Electrospinning Source. *Nano Lett.* **2004**, *4*, 2105−2108.
(18) Pinto, N.; Johnson, J. A. T., Jr.; MacDiarmid, A. G.; Mueller, C. H.; Theofylaktos, N.; Robinson, D. C.; Miranda, F. A. Electrospun Polyaniline/Polyethylene Oxide Nanofiber Field-Effect Transistor. *Appl. Phys. Lett.* **2003**, *83*, 4244−4246.
(19) Matthews, J. A.; Wnek, G. E.; Simpson, D. G.; Bowlin, G. L. Electrospinning of Collagen Nanofibers. *Biomacromolecules* **2002**, *3*, 232−238.
(20) Li, W. J.; Laurencin, C. T.; Caterson, E. J.; Tuan, R. S.; Ko, F. K. Electrospun Nanofibrous Structure: A Novel Scaffold for Tissue Engineering. *J. Biomed. Mater. Res.* **2002**, *60*, 613−621.
(21) Sun, Y.; Seo, J. H.; Takacs, C. J.; Seifer, J.; Heeger, A. J. Inverted Polymer Solar Cells Integrated with a Low-Temperature-Annealed Sol−Gel-Derived ZnO Film as an Electron Transport Layer. *Adv. Mater.* **2011**, *23*, 1679−1683.
(22) Kyaw, A. K. K.; Sun, X. W.; Jiang, C. Y.; Lo, G. Q.; Zhao, D. W.; Kwong, D. L. An Inverted Organic Solar Cell Employing a Sol−Gel Derived ZnO Electron Selective Layer and Thermal Evaporated MoO_3 Hole Selective Layer. *Appl. Phys. Lett.* **2008**, *93*, 221107.
(23) White, M. S.; Olson, D. C.; Shaheen, S. E.; Kopidakis, N.; Ginley, D. S. Inverted Bulk-Heterojunction Organic Photovoltaic Device Using a Solution-Derived ZnO under Layer. *Appl. Phys. Lett.* **2006**, *89*, 143517.
(24) Waldauf, C.; Morana, M.; Denk, P.; Schilinsky, P.; Coakley, K.; Choulis, S. A.; Brabec, C. J. Highly Efficient Inverted Organic Photovoltaics Using Solution Based Titanium Oxide as Electron Selective Contact. *Appl. Phys. Lett.* **2006**, *89*, 233517.
(25) Song, M. Y.; Kim, D. K.; Ihn, K. J.; Jo, S. M.; Kim, D. Y. Electrospun TiO_2 Electrodes for Dye-Sensitized Solar Cells. *Nanotechnology* **2004**, *15*, 1861−1865.
(26) Onozuka, K.; Ding, B.; Tsuge, Y.; Naka, T.; Yamazaki, M.; Sugi, S.; Ohno, S.; Yoshikawa, M.; Shiratori, S. Electrospinning Processed Nanofibrous TiO_2 Membranes for Photovoltaic Applications. *Nanotechnology* **2006**, *17*, 1026−1031.
(27) Fujihara, K.; Kumar, A.; Jose, R.; Ramakrishna, S.; Uchida, S. Spray Deposition of Electrospun TiO_2 Nanorods for Dye-Sensitized Solar Cell. *Nanotechnology* **2007**, *18*, 365709.
(28) Jose, R.; Kumar, A.; Thavasi, V.; Ramakrishna, S. Conversion Efficiency Versus Sensitizer for Electrospun TiO_2 Nanorod Electrodes in Dye-Sensitized Solar Cells. *Nanotechnology* **2008**, *19*, 424004.
(29) Ghadiri, E.; Taghavinia, N.; Zakeeruddin, S. M.; Gratzel, M.; Moser, J. Enhanced Electron Collection Efficiency in Dye-Sensitized Solar Cells Based on Nanostructured TiO_2 Hollow Fibers. *Nano Lett.* **2010**, *10*, 1632−1638.
(30) Shim, H.-S.; Kim, J. W.; Kim, W. B. Fabrication and Optical Properties of Conjugated Polymer Composited Multi-Arrays of TiO_2 Nanowires via Sequential Electrospinning. *J. Nanosci. Nanotechnol.* **2009**, *9*, 4721−4726.
(31) Shim, H.-S.; Kim, J. W.; Sung, Y.-E.; Kim, W. B. Electrochromic Properties of Tungsten Oxide Nanowires Fabricated by Electrospinning Method. *Sol. Energy Mater. Sol. Cells* **2009**, *93*, 2062−2068.
(32) Kim, Y. S.; Yu, B. K.; Kim, D.-Y.; Kim, W. B. A Hybridized Electron-Selective Layer Using Sb-doped SnO_2 Nanowires for Efficient Inverted Polymer Solar Cells. *Sol. Energy Mater. Sol. Cells* **2011**, *95*, 2874−2879.
(33) Jha, A. R. *Infrared Technology: Applications to Electro-optics, Photonic Devices, and Sensors*; John Wiley & Sons: New York, 2000; p 23.
(34) Yu, G.; Pakbaz, K.; Heeger, A. J. Semiconducting Polymer Diodes: Large Size, Low Cost Photodetectors with Excellent Visible−Ultraviolet Sensitivity. *Appl. Phys. Lett.* **1994**, *64*, 3422−3424.
(35) Deng, X. Y.; Zheng, L. P.; Mo, Y. Q.; Yu, G.; Yang, W.; Weng, W. H.; Cao, Y. Efficient Polymer Photovoltaic Devices Based on Polymer D−A Blends. *Chin. J. Polym. Sci.* **2001**, *19*, 597−602.
(36) Yu, G.; Srdanov, G.; Wang, H.; Cao, Y.; Heeger, A. J. High-Performance Polymer Photovoltaic Cells and Photodetectors. *Proc. SPIE* **2001**, *4108*, 48−56.
(37) Shim, H. S.; Na, S. I.; Nam, S. H.; Ahn, H. J.; Kim, H. J.; Kim, D. Y.; Kim, W. B. Efficient Photovoltaic Device Fashioned of Highly Aligned Multilayers of Electrospun TiO_2 Nanowire Array with Conjugated Polymer. *Appl. Phys. Lett.* **2008**, *92*, 183107.
(38) Meng, F. X.; Shen, L.; Wang, Y. F.; Wen, S. P.; Gu, X. H.; Zhou, J. R.; Tian, S.; Ruan, S. P. An Organic−Inorganic Hybrid UV Photodetector Based on a TiO_2 Nanobowl Array with High Spectrum Selectivity. *RSC Adv.* **2013**, *3*, 21413−21417.
(39) Deng, M. J.; Shen, S. L.; Wang, X. W.; Zhang, Y. J.; Xu, H. R.; Zhang, T.; Wang, Q. B. Controlled Synthesis of $AgInS_2$ Nanocrystals and Their Application in Organic−Inorganic Hybrid Photodetectors. *Cryst. Eng. Commun.* **2013**, *15*, 6443−6447.